Desalination and Water Treatment
www.deswater.com
doi: 10.5004/dwt.2023.29728

300 (2023) 213–229
July

Synthesis of graphene oxide–magnesium oxide composites and cationic dyes removal from water

Narges Behzad[a], Omid Moradi[b,*], Heydar Raissi[c], Mohammad Hakimi[a], Shahla Mozaffari[a]

[a]*Department of Chemistry, Payame Noor University, 19395-4697 Tehran, Iran, emails: narges.behzad@student.pnu.ac.ir (N. Behzad), m.hakimi@pnu.ac.ir (M. Hakimi), sh_mozafari@pnu.ac.ir (S. Mozaffari)*
[b]*Department of Chemistry, Shahr-e-Qods Branch, Islamic Azad University, Tehran, Iran, email: o.moradi@qodsiau.ac.ir/ moradi.omid@gmail.com*
[c]*Chemistry Department, University of Birjand, Birjand, Iran, email: hraeisi@birjand.ac.ir*

Received 14 March 2023; Accepted 20 June 2023

ABSTRACT

Herein, graphene oxide (GO)–magnesium oxide (MgO) nanocomposites (GO-MgO) (GO1.5MgO, GO3MgO, GO4.5MgO, and GO6MgO) were synthesized and characterized. Methylene blue (MB) and crystal violet (CV) as cationic dyes were used as contaminants. The results showed that MB and CV adsorption followed pseudo-second-order kinetics. The isotherm data indicated that MB and CV removal obeyed the Langmuir isotherm model. It means that the adsorption process was carried out in specific homogeneous sites on the adsorbent surface. The adsorption thermodynamic data presented that the negative ΔG of CV and MB removal by the synthesized adsorbents presented physical and spontaneous adsorption. Also, the positive values of ΔH and ΔS showed the endothermic properties of adsorption and the increase of dye irregularity on the adsorbent surface. The amount of dye adsorbed on the synthesized adsorbents increases by increasing the contaminant concentration. The results indicated that contaminant adsorption capacity enhances by enhancing the adsorbent dose and then decreases to some extent. As the adsorbent dose increases, the active sites will be more accessible. The adsorbent particles are agglomerated at values higher than the optimal value of the adsorbent dose. Thus dye removal is reduced. It can be concluded that the synthesized GO-MgO nanocomposites could be used as alternative adsorbents to remove cationic dyes.

Keywords: Graphene oxide–magnesium oxide composite; Synthesis; Cationic dyes; Adsorption; Colored wastewater

1. Introduction

The high speed of industrialization has caused our water resources to be in danger of destruction and deterioration. A huge range of toxic and dangerous substances are constantly being released into the waters. One of the causes of this issue can be the lack of effective control of the output flow in the production source. Among these cases, synthetic dyes have attracted a lot of attention due to the estimated release of 280 thousand tons annually into the environment. According to the information from the World Bank, 17%–20% of the share of industrial water pollution originates from the purification and dyeing processes of textile industries. Due to their inherent properties, dyes are easily observed even in low concentrations in polluted waters. The complex aromatic structure along with their synthetic origin has made these substances to be in stable form and difficult to biodegrade. By preventing the passage of light, dyes can affect the photosynthetic activity (by reflection and adsorption of sunlight), hence they can cause disturbances in the ecology of receiving waters. Some dyes are highly toxic, carcinogenic, and mutagenic in nature and can even accumulate naturally in the food cycle. Therefore, it can be said that the direct release of colored

* Corresponding author.

wastewater into the aquatic ecosystem is both environmentally unsafe and visually unacceptable [1–6].

Textile dyes can increase the environmental pollution potential. About 50% of the dyes available in the market are azo dyes that have an azo bond (–N=N–). Azo dyes are found in different acidic, basic, direct, and dispersed groups. Some of them and their raw materials are carcinogenic to human because they produce toxic aromatic amines. About 1%–20% of the total global production of dyes is removed from the cycle during the dyeing process and released into the effluent. In addition, other compounds such as polyacrylates, phosphonates, and anti-clotting agents may be present in the textile wastewater. In order to maintain the ecological balance, it is necessary to remove dyes from textile wastewater. Applying conventional methods of colored wastewater treatment has become a big challenge for engineers due to the existing strict laws on the quality of the effluent. Some dyes are composed of non-biodegradable substances, which has caused the common methods of biological treatment to be ineffective due to the resistance of some dyes to decomposition [7–11]. Therefore, it seems necessary to find a suitable and effective solution for the complete removal of the dye molecules.

The removal of dyes by the adsorption process has many advantages such as very low operating costs, simple operating conditions, etc. This process is one of the leading processes in the treatment of wastewater in industrial sectors, domestic activities, municipalities, agricultural activities, hospitals, etc. Currently, the adsorption process is considered a green method [12].

In recent years, we have seen a lot of progress in the study of graphene-based materials (the first atomic crystal available in atomic form), along with significant measures in the mass production of this material. These material with the thickness of one carbon atom uniquely shows its characteristics such as very high mechanical resistance, special thermal and electronic conductivity, high adsorption capacities, etc. These features have made these materials become a very attractive material for various applications [13]. Inorganic nanoparticles can improve various properties of polymer matrices such as density and thermal stability, and this can open the way for more applications. For example, MgO nanoparticles have applications in various fields and can act as excellent catalysts and absorbers. Also, these nanoparticles can have antibacterial properties [14].

Several dye adsorbents such as clay nanocomposite (clay/GO/Fe_2O_3) (for removing methylene blue) [15], Fe_3O_4 or γ-Fe_2O_3 coated multi-wall carbon nanotube methylene blue (MB, neutral red, and brilliant cresyl blue) [16], Magnetic (γ-Fe_2O_3) sugarcane bagasse activated carbon (MB) [17], ZnO: Cr-AC (malachite green (MG), eosin yellow, and auramine O) [18], Konjac glucomannan/graphene oxide (KGM/GO) sponges (MG) [19], Cobalt iron oxide nanoparticles functionalized hydrazine (CoFeNPs) (amaranth, naphthol blue black, acid orange 7, reactive orange 16, and acid orange 52) [20] were synthesized and used.

A literature review presented that cationic dye removal using graphene oxide (GO)–magnesium oxide (MgO) nanocomposites (GO-MgO) was not investigated in detail. Herein, GO-MgO nanocomposites (GO1.5MgO, GO3MgO, GO4.5MgO, and GO6MgO) were synthesized, characterized and used to remove methylene blue (MB) and crystal violet (CV) as cationic dyes. The kinetics, isotherm, and thermodynamics of MB and CV removal by the synthesized adsorbents were studied. Also, the effects of pollutant concentration, solution pH, and adsorbent dosage on MB and CV adsorption were investigated.

2. Experimental set-up

2.1. Materials

Graphite powder, H_2SO_4, $KMnO_4$, sodium nitrate, H_2O_2, HCl, sodium hydroxide, and magnesium nitrate were obtained from Merck. Methylene blue and crystal violet were achieved from Sigma-Aldrich. The materials were used as obtained without any purification.

2.2. Synthesis

2.2.1. Graphene oxides (GOs)

GO nanosheets were synthesized in water by the modified Hummer method. For this purpose, 1 g of expanded graphite powder was stirred in 120 mL of concentrated sulfuric acid for 2 h. In the next step, 1.5, 3, 4.5, and 6 g of potassium permanganate and 1 g of sodium nitrate were gradually added to the solution to prepare GO1.5, GO3, GO4.5, and GO6 samples. The mixing of the solution was carried out for 72 h. After diluting the solution with 600 mL of deionized water, 5 mL of H_2O_2 was added to end the oxidation reaction. With this, the mixture color changed from brownish-green to yellow, which indicates the end of the reaction. The mixture was kept motionless and stable in a corner for 24 h to precipitate, and then centrifuged for two min at 4,000 rpm and the mixture was washed using 1 molar HCl and deionized water three times.

2.2.2. Graphene oxide (GO)–magnesium oxide (MgO) (GO-MgO)

0.1 g of the synthesized GO was dispersed in 100 mL of distilled water using ultrasound. Then the solution pH was adjusted to 7 using NaOH. 0.2 g of magnesium nitrate salt was added. The solution was placed on the stirrer at room temperature for 30 min and then transferred to the autoclave. The autoclave was placed in the oven for 24 h at a temperature of 80°C (hydrothermal reaction and synthesis of magnesium oxide on the surface of graphene oxide sheets). According to the type of graphene oxide used in this reaction, 4 samples of modified graphene oxide plates were synthesized (GO1.5MgO, GO3MgO, GO4.5MgO, and GO6MgO). After 24 h, they were centrifuged and washed using deionized water three times.

2.3. Characterization

The material morphology was investigated by the field-emission scanning electron microscopy model TESCAN MIRA 3. The Brunauer–Emmett–Teller (BET) surface area analysis of material was performed by BELSORP-mini II (Japan). The zeta potential of the nanomaterials was investigated using ZETASIZER Nano-NS through

Malvern instrument. The thermal gravimetric analysis (TGA) was performed by the Mettler Toledo machine in the temperature range of 25°C–600°C. The amount of dye was measured using double beam UV-Vis spectrometry (model CECIL 9000).

2.4. Dye adsorption

To study the adsorption of dyes with synthesized adsorbents, solutions (100 mL) containing 10 mg of adsorbent with pollutants (40 mg/L) were prepared at various pHs (3–11). The optimal amount of adsorbents (0.005–0.015 g) was measured in the solution with the same laboratory conditions mentioned above and at the optimal pH. The experiments were done with pollutants concentrations from 10 to 80 mg/L, the time of the adsorption process (from 5 to 120 min) and the temperature of the solution (15°C, 25°C, and 35°C), and the optimal conditions obtained. After the adsorption process, the sample was centrifuged to separate adsorbent particles. The concentration of the unadsorbed dye in the remaining solution after centrifugation was measured using UV-Vis spectroscopy using Eqs. (1) and (2).

$$q_e = \frac{\left(C_0 - C_e\right) \times V}{m} \tag{1}$$

$$\text{Removal}(\%) = \frac{C_0 - C_e}{C_0} \tag{2}$$

where C_0, C_e, q_e, V, m, and R represent the initial pollutant concentration (mg/L), equilibrium concentration (mg/L), adsorption capacity (mg/g), the volume of solution (L), amount of adsorbent (g) and removal efficiency (%), respectively.

3. Results and discussion

3.1. Characterization

3.1.1. Scanning electron microscopy

The morphology of materials is studied by scanning electron microscopy (SEM) images. Fig. 1 shows the SEM images of synthesized adsorbents including GO1.5MgO, GO3MgO, GO4.5MgO, and GO6MgO. Due to the strong interplanar reaction, GO layers are no longer similar to flat and straight graphite sheets. The edges and plates of GO are curved and rough, this issue was also observed in other research [20,21]. The addition of magnesium oxide to graphene oxide causes surface changes in the form of a porous, uneven, and irregular surface to be observed in graphene oxide. It was found that the twisted GO layer and well-dispersed MgO were anchored on the graphene oxide sheets. This issue was also observed in other research including TiO_2/graphene oxide nanocomposites [22]. In general, the GO has a thin layer structure and irregular shape. It shows multilayer structures because of the presence of oxidizing functional groups. The special layered structure of GO shows that it was beneficial for the growth of MgO.

3.1.2. Brunauer–Emmett–Teller

The porosity of GO-based nanocomposite can be studied using BET analysis. Herein surface area of the synthesized GO-based adsorbents was measured (Table 1). The results indicated that the BET surface area of GO1.5MgO, GO3MgO, GO4.5MgO, and GO6MgO was 196.5, 482.3, 398.7, and 542.36 m^2/g, respectively. The data showed that the surface area increased by increasing MgO. It can be attributed that the MgO prevents the accumulation of graphene oxide layers. Increasing the surface area increases the ability to adsorb pollutants by adsorption in the water environment [22,23].

3.1.3. Thermal gravimetric analysis

The TGA is used to determine the thermal stability of different materials. The thermogravimetric analysis measures the weight loss of materials. Fig. 2 presents that the thermal stability of GO composites was investigated by TGA analysis at air environment. The results show that GO is degraded in three stages. The first and second stages of weight loss are at 50°C–120°C (loss of water molecules) and at 120°C–440°C in (loss of oxygen-containing groups), respectively. The third stage above 440°C is related to the remaining unstable carbon in the structure and destruction due to the heat of oxygen functional groups in the original structure. It is for the production of CO and CO_2 [24–26]. The increase in GO nanocomposite thermal stability can be attributed to two reasons. MgO nanoparticle has higher thermal stability. Thus, the MgO presence in the composite may make it more stable thermally. Also, the MgO interacts with GO through the functional groups such as OH and COOH available in the GO surface [14].

3.1.4. Zeta potential

When the adsorbent surface charge is positive, it can adsorb pollutant molecules with a negative charge. Also, when the adsorbent surface charge is negative, it will adsorb the pollutant with a positive charge. The surface charge of the material is measured using a zeta potential analyzer. Fig. 3 shows the zeta potential of the synthesized adsorbents at different pH values. The results show that GO1.5MgO, GO3MgO, GO4.5MgO, and GO6MgO have a zeta potential of +4.4, –2.4, –10.3, and –17.8 mV. These results can be because of the presence of more functional groups on the surface of the synthesized nanocomposite.

3.2. Dyes removal

3.2.1. Adsorption kinetics

Adsorption kinetics models provide useful information about the interactions between the adsorbed pollutant molecule and the adsorbent, and the parameters affecting the adsorption rate [27–32].

The pseudo-first-order (Fig. 4) [Eq. (3)] is based on adsorption due to the concentration difference between the adsorbent surface and the pollutant molecule. Therefore, this process takes place only with the external mass transfer coefficient [29].

$$\log\left(q_e - q_t\right) = \log q_e - \frac{k_1 t}{2.303} \tag{3}$$

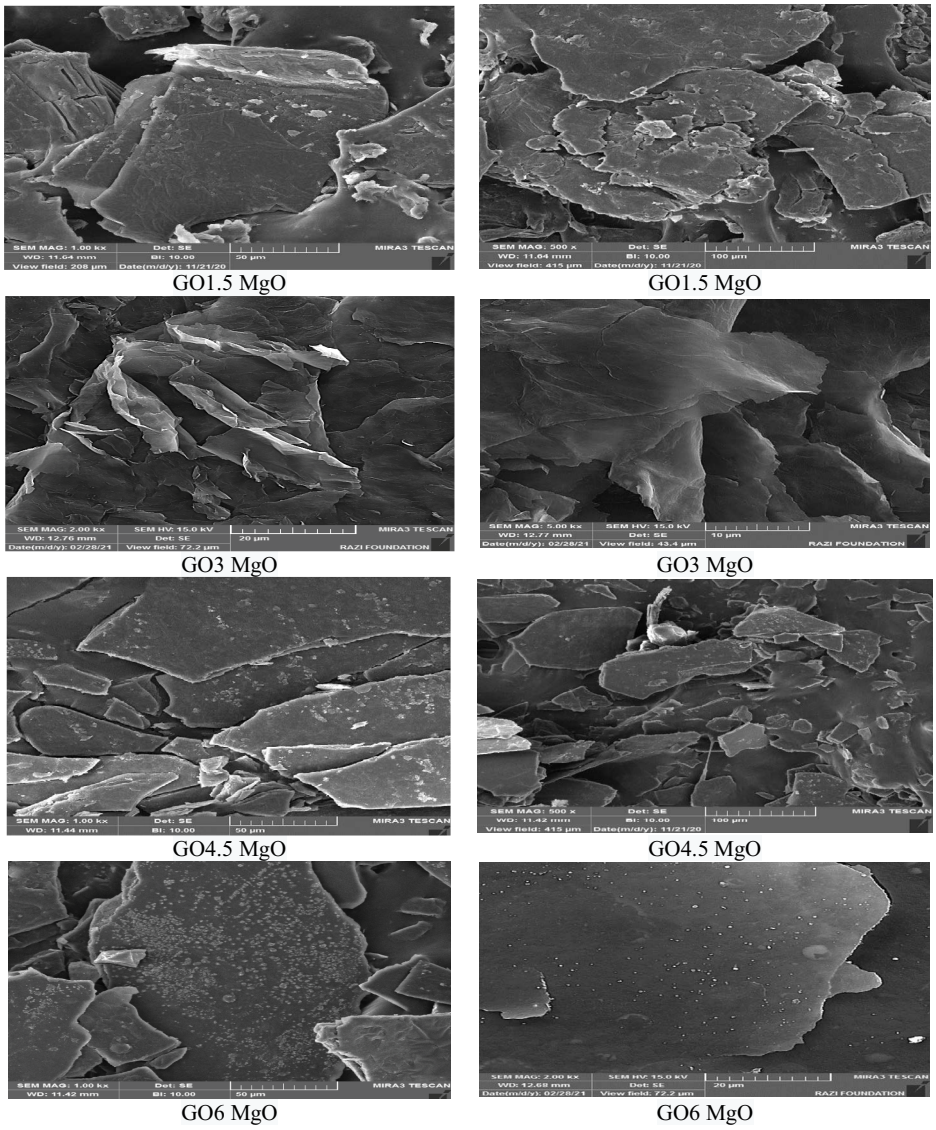

Fig. 1. Scanning electron microscopy images of the synthesized adsorbents (GO1.5MgO, GO3MgO, GO4.5MgO, and GO6MgO).

Table 1
Brunauer–Emmett–Teller of the synthesized adsorbents (GO1.5MgO, GO3MgO, GO4.5MgO, and GO6MgO)

Adsorbent	Mean pore diameter (nm)	Total pore diameter (cm^3/g)	$a_{s,BET}$ (m^2/g)
GO1.5MgO	1.1254	0.1137	196.5
GO3MgO	2.6741	0.3715	482.3
GO4.5MgO	1.9634	0.3822	398.7
GO6MgO	4.2347	0.5186	542.36

In the pseudo-second-order (Fig. 5) [Eq. (4)], the rate of adsorption is proportional to the square of vacant sites. It is obtained by integrating from the sides and applying the following boundary conditions [31].

$$\frac{t}{q_t} = \frac{1}{k_2 q_e^2} + \left(\frac{1}{q_e}\right) t \quad (4)$$

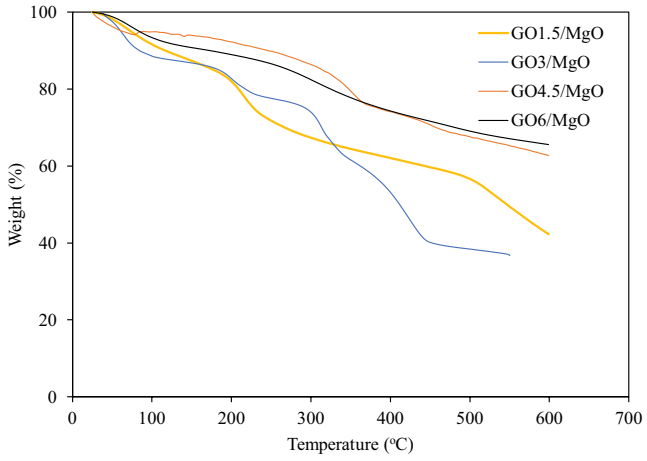

Fig. 2. Thermal gravimetric analysis of the synthesized adsorbents (GO1.5MgO, GO3MgO, GO4.5MgO, and GO6MgO).

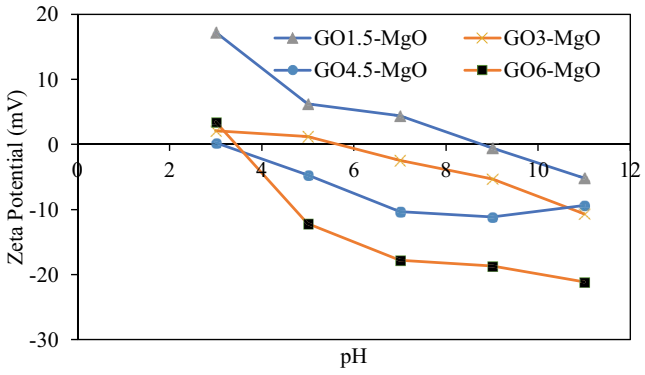

Fig. 3. Zeta potential of the synthesized adsorbents (GO1.5MgO, GO3MgO, GO4.5MgO, and GO6MgO).

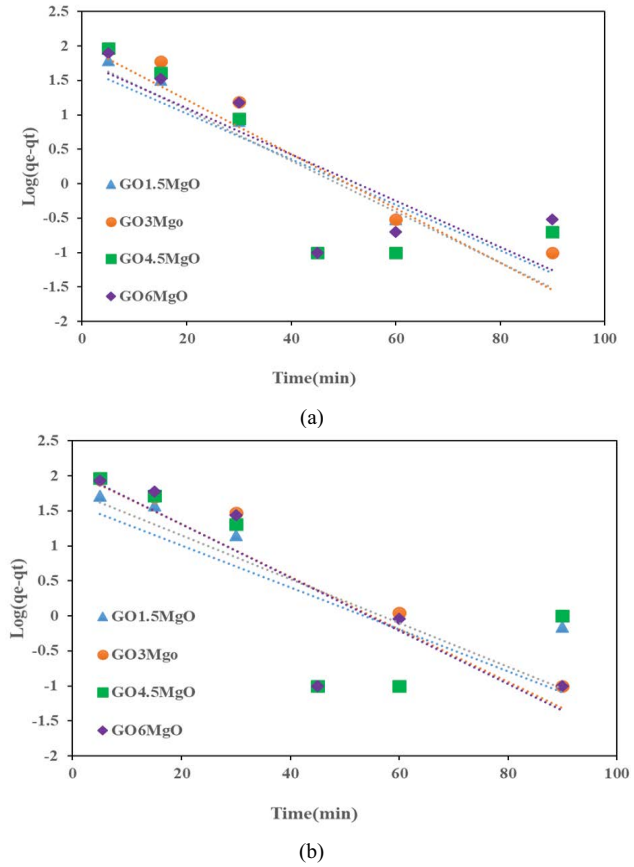

Fig. 4. Pseudo-first-order of dye adsorption by the synthesized adsorbents (GO1.5MgO, GO3MgO, GO4.5MgO, and GO6MgO) (a) MB and (b) CV.

The intraparticle diffusion model (Fig. 6) is studied by the following equation [32].

$$q_t = k_p t^{0.5} + I \tag{5}$$

where I (mg/g) is the intercept and k_p (mg/g·min$^{1/2}$) is the slope and represents the permeation rate constant inside the adsorbent. The I value gives useful information

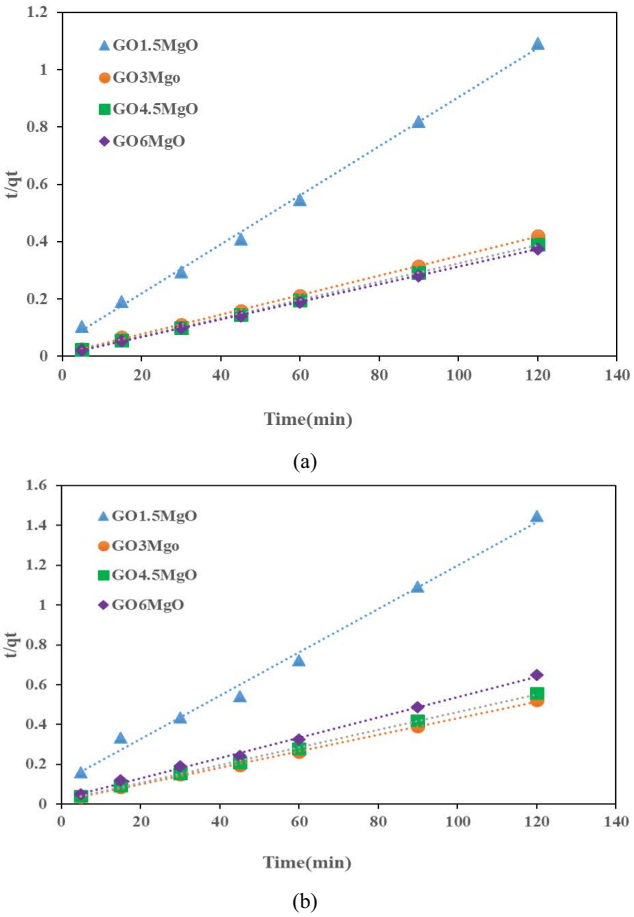

Fig. 5. Pseudo-second-order of dye adsorption by the synthesized adsorbents (GO1.5MgO, GO3MgO, GO4.5MgO, and GO6MgO) (a) MB and (b) CV.

about the thickness of the boundary layer: the greater the thickness, the greater the effect of the boundary layer [32].

Herein, kinetic models (Figs. 4–6) were used to investigate the adsorption process. The selection of the dominant system in the process was done by comparing the determined coefficient (R^2) of the models. The results in Table 2 indicated that MB and CV removal follows pseudo-second-order. It means that the adsorption process depends on pollutant concentration and adsorbent dosage.

3.2.2. Adsorption isotherms

It becomes possible to describe the reaction of adsorbent and adsorbate (organic pollutant) with adsorption isotherms. The adsorbent surface may act as a single layer or multiple layers. The different isotherm models are used to study the adsorption isotherm in this treatise [27,33–37].

The Langmuir adsorption isotherm [Eq. (4)] (Fig. 7) is the simplest one for monolayer adsorption in liquid solutions, which is based on several assumptions:

- Adsorption is carried out in specific homogeneous areas of the adsorbent.
- The adsorption sites present in the adsorbent are the same.

- Each of the adsorption sites is able to adsorb only one adsorbed molecule.
- The adsorbent has a certain capacity to adsorb the pollutant.
- All the adsorption sites in the adsorbent have equivalent energy, that is, the adsorbents are identical in structure [27].

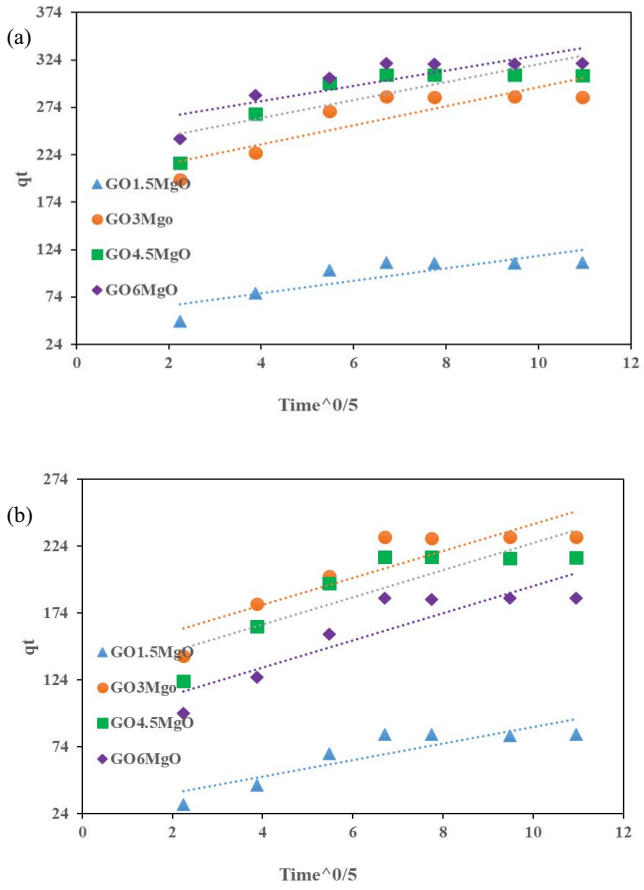

Fig. 6. Intraparticle diffusion of dye adsorption by the synthesized adsorbents (GO1.5MgO, GO3MgO, GO4.5MgO, and GO6MgO) (a) MB and (b) CV.

$$\frac{C_e}{q_e} = \left(\frac{1}{Q_0 K_L}\right) + \left(\frac{C_e}{Q_0}\right) \tag{6}$$

Freundlich isotherm [Eq. (7)] (Fig. 8) predicts that by increasing the initial concentration of the dye in the solution, the adsorption rate of the dye will increase. The Freundlich equation is presented as follows [37]:

$$\log q_e = \log K_F + \left(\frac{1}{n}\right)\log C_e \tag{7}$$

The Temkin isotherm (Fig. 9) is used to interpret the interactions between the adsorbent and the adsorbate. In this model, ignoring very low or very high pollutant concentrations, the contaminant adsorption heat diminishes linearly with the surface coverage due to the adsorbate–adsorbent interaction. The equation of the Temkin isotherm is as follows [37]:

$$q_e = B_T \ln A_T + B_T \ln C_e \tag{8}$$

Herein, the isotherm models (Figs. 7–9) were used to study the adsorption process. The selection of the dominant system in the process was done by comparing the determined coefficient (R^2) for each of the models. The results in Table 3 indicated that MB and CV removal follows the Langmuir isotherm model. It means that the adsorption process was carried out in specific homogeneous sites on the adsorbent surface.

3.2.3. Adsorption thermodynamics

In the adsorption process, it is interesting to investigate the pollutant transfer from one phase to another and how it is distributed between phases in the state of composition. In most cases, pollutants are transferred from one phase to another. The study of mass transfer for each pollutant is determined by the chemical potentials. The chemical potential is the Gibbs free energy (ΔG, J/mol) of the pollutant in the superior phases [38–40]. The ΔG, entropy (ΔS: J/mol·K), and enthalpy (ΔH: J/mol) are obtained using the following equations:

Table 2
Kinetics parameters of dye (MB and CV) adsorption by the synthesized adsorbents (GO1.5MgO, GO3MgO, GO4.5MgO, and GO6MgO) (k_1 (min^{-1}), q (mg/g), and k_1 (g/min·mg))

Dye	Adsorbent	Pseudo-first-order			Pseudo-second-order			Intraparticle diffusion		
		q	k_1	R^2	q	k_2	R^2	k_p	I	R^2
MB	GO1.5	48	0.0763	0.7228	116	0.0016	0.9979	6.5558	52	0.7080
	GO3	100	0.0906	0.7807	293	0.0013	0.9993	10.0375	195	0.7458
	GO4.5	65	0.0851	0.7163	314	0.0017	0.9997	9.4060	225	0.6705
	GO6	58	0.0772	0.6741	325	0.0019	0.9998	8.0897	248	0.7050
CV	GO1.5	40	0.0689	0.5509	92	0.0011	0.9924	6.1861	27	0.7766
	GO3	113	0.0861	0.7418	240	0.0011	0.9989	10.0048	140	0.7845
	GO4.5	60	0.0720	0.5275	224	0.0011	0.9989	10.1361	125	0.7432
	GO6	116	0.0873	0.7507	196	0.0009	0.9976	10.1605	93	0.7925

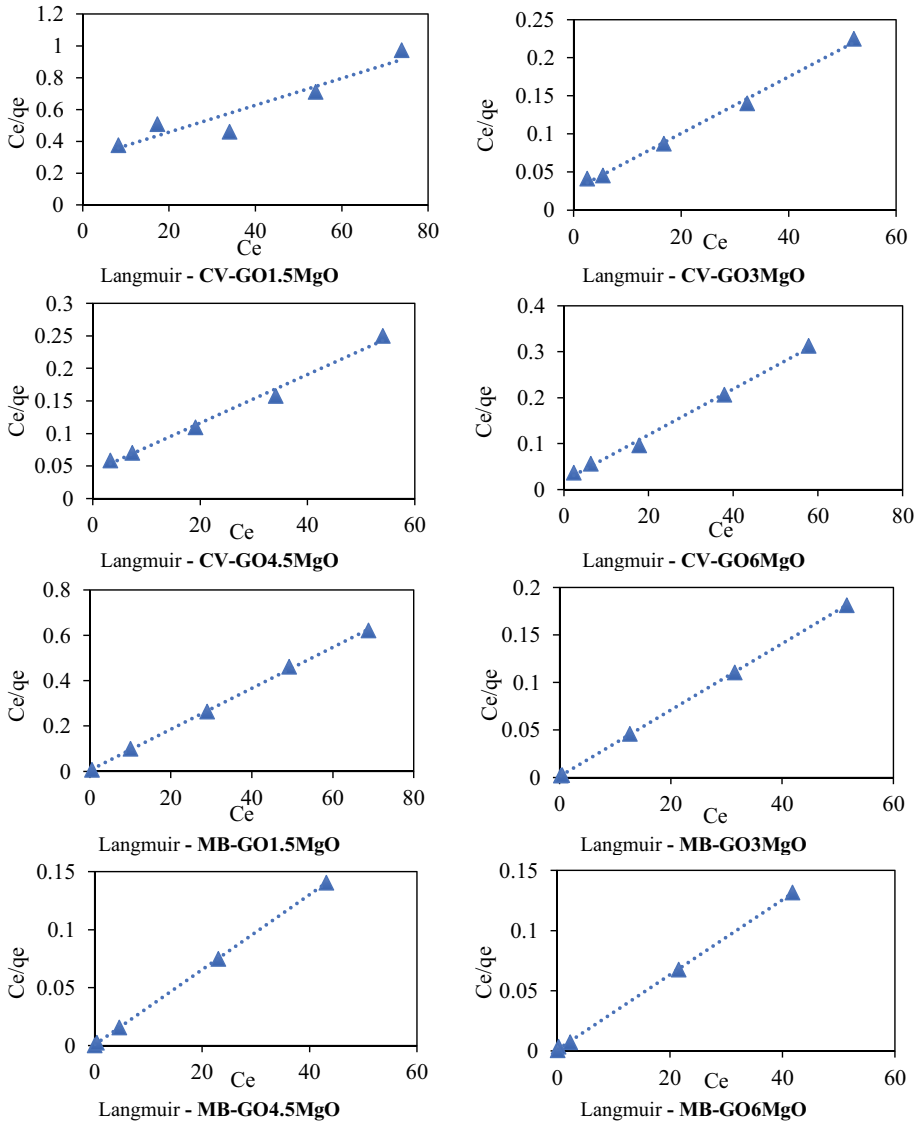

Fig. 7. Langmuir isotherm of dye (CV and MB) adsorption by the synthesized adsorbents (GO1.5MgO, GO3MgO, GO4.5MgO, and GO6MgO).

$$K_d = \frac{q_e}{C_e} \tag{9}$$

$$\ln K_d = \frac{\Delta S}{R} - \frac{\Delta H}{RT} \tag{10}$$

$$\Delta G = \Delta H - T\Delta S \tag{11}$$

Dye removal experiments were performed at temperatures of 288, 298, and 308 K to investigate its effect on CV and MB adsorption (Fig. 10). The $\ln K_d$ vs. $1/T$ was presented in Fig. 10. ΔG value was –1,505.4; –3,198.4 and –4,891.4 J/mol (GO1.5MgO), –5,153; –6,083 and –7,013 J/mol (GO3MgO), –5,200.8; –6,386.8 and –7,572.8 J/mol (GO4.5MgO), and –5,922.2; –6,796.2 and –7,670.2 J/mol (GO6MgO) for CV dye and –373.6; –2,050.6 and –3,727.6 J/mol (GO1.5MgO), –3,949.2; –4,883.2 and –5,817.2 J/mol (GO3MgO), –3,865.4; –4,658.4 and –5,451.4 J/mol (GO4.5MgO), and –4,219; –5,724 and –7,229 J/mol (GO6MgO) for MB at 288, 298, and 308 K (Table 4). The negative ΔG of CV and MB removal confirmed the spontaneous and physical adsorption. The positive values of ΔH and ΔS, respectively indicate the endothermic properties of adsorption and the increase of dye irregularity on the adsorbent surface.

3.2.4. Effect of pollutant concentration

The contaminant concentration effect on dye removal was investigated in detail. The MB and CV cationic dyes concentration effect on the equilibrium adsorption capacity was investigated (Fig. 11). The dye removal ability increases by enhancing the cationic dye concentration from 10 to 80 mg/L. The cause of this phenomenon is the enhancing driving force of the concentration gradient at higher initial contaminant concentration. The removal of dye by the adsorbent is rapid and reaches equilibrium rapidly due to

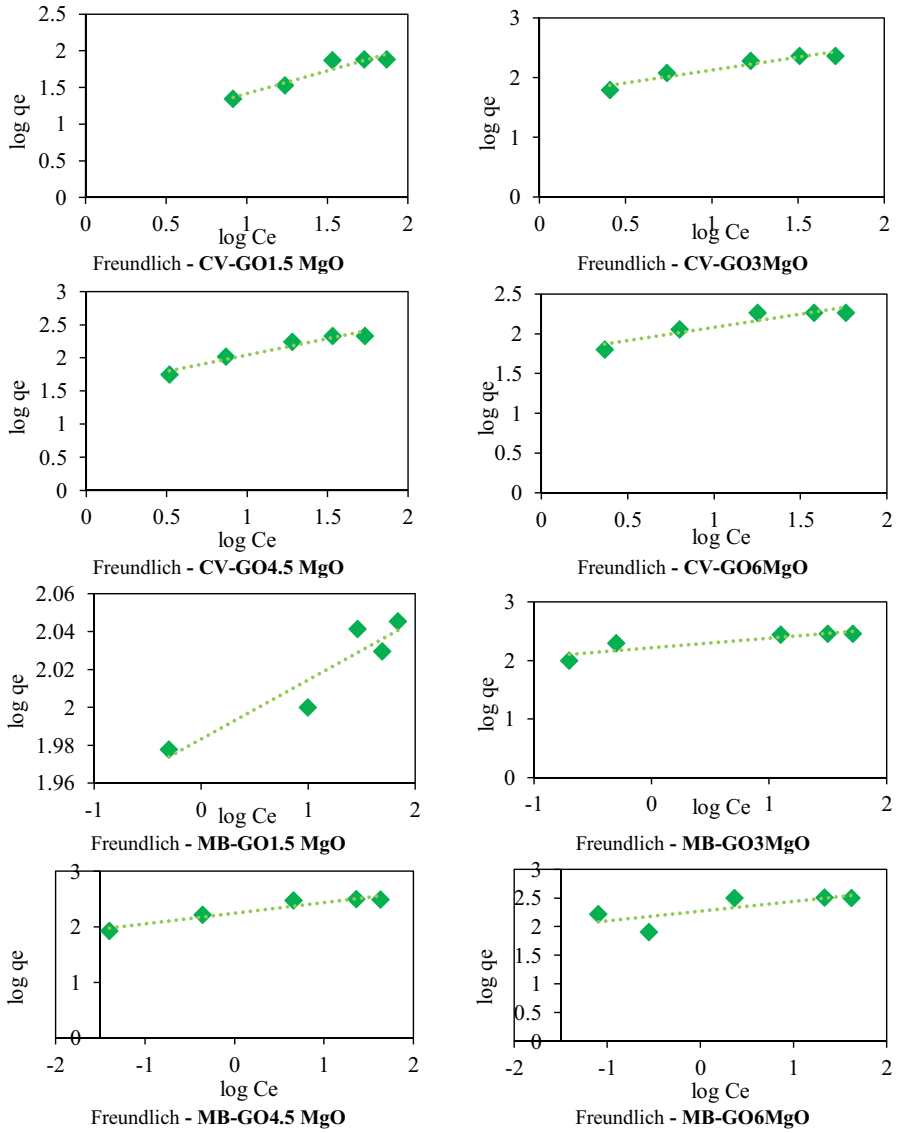

Fig. 8. Freundlich isotherm of dye (CV and MB) adsorption by the synthesized adsorbents (GO1.5MgO, GO3MgO, GO4.5MgO, and GO6MgO).

the forming of a single-layer coating of molecules on the outer surface of the adsorbent. The number of adsorption sites diminishes at higher contaminant concentrations. It is unlikely that the contaminant is adsorbed in only one layer at the adsorbent external surface. In fact, the diffusion of exchange molecules in the adsorbent surface may control the extent of adsorption [29–32].

3.2.5. Effect of the solution pH

The solution pH effect on contaminant removal was studied in detail. To get more information about the pH effect on removal efficiency, experiments have been carried out in the range of pH = 3–11, which can be seen in Fig. 12. Dye removal by GO1.5MgO, GO3MgO, and GO4.5MgO was not changed considerably by the solution pH. It can be concluded that it was not carried out by electrostatic attraction. Pollutant removal by GO6MgO increased by solution pH. Under acidic conditions (pH = 3), the adsorption site was accumulated by proton and positively charged. MB and CV are cationic dyes with a positive charge. Thus, electrostatic repulsion occurs between the surface of adsorbents and dye molecules. Also, protons competing with the cationic dyes and contaminant removal reduces [27]. The zeta potential of the GO6MgO adsorbent starts to become negative at pH > 5. It causes to increase in the removal of the cationic dyes (MB and CV).

3.2.6. Adsorbent dose effect

To evaluate the adsorbent dose effect, the dose of adsorbents was examined in the range of 0.005–0.015 g. Reactors of 100 mL of dye (MB and CV) solution (40 mg/L) were stirred for 100 min at room temperature. Fig. 13 shows the removal of MB and CV by the adsorbents and the value of q_e in different amounts of adsorbent were presented. The

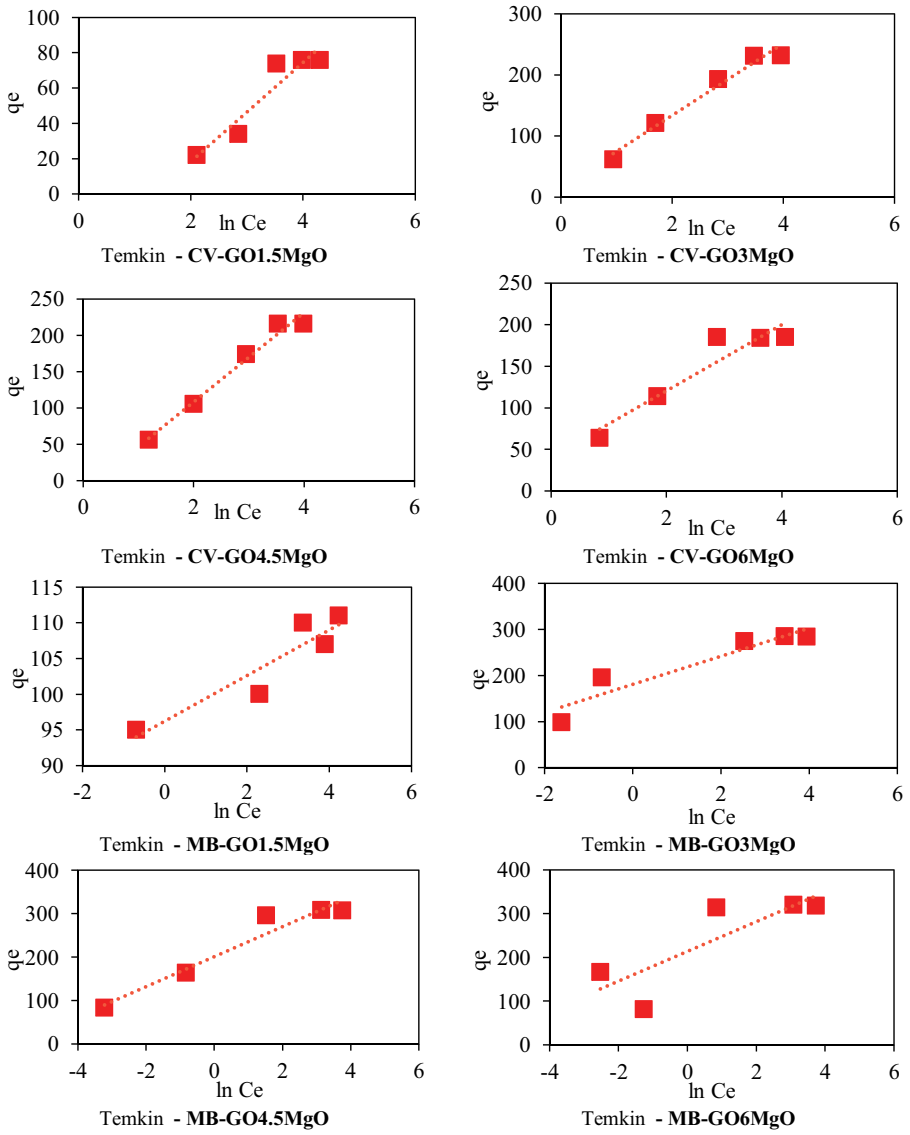

Fig. 9. Temkin isotherm of dye (CV and MB) adsorption by the synthesized adsorbents (GO1.5MgO, GO3MgO, GO4.5MgO, and GO6MgO).

adsorption capacity of different adsorbents for 0.005, 0.008, 0.010, 0.012, and 0.015 g was 73, 95, 110, 100, and 104 mg/g for GO1.5MgO, 210, 253, 274, 261, and 257 for GO3MgO, 272, 275, 283, 295, and 264 for GO4.5MgO and 269, 287, 310, 314, and 261 mg/g for GO6MgO, respectively. The results indicated that dye adsorption capacity increases by increasing the adsorbent dose and then decreases to some extent. As the adsorbent dose increases, the active sites of the adsorbent surface will be more accessible [33–36]. At values higher than the optimal value of the adsorbent dose, the particles are agglomerated, as a result, the amount of dye removal reduced.

3.2.7. Salt effect

The presence of charged electrolytes in dye-containing wastewater enables us to study the effect of foreign ions on dye adsorption. Herein, the effect of sodium sulphate on MB and CV removal was investigated (Fig. 14). Dye adsorption capacity of GO1.5MgO, GO3MgO, GO4.5MgO, and GO6MgO without salt (0 g/L of sodium sulphate) was 100, 261, 295, and 314 mg/g for MB and 57, 211, 212, and 185 mg/g for CV, respectively. The presence of sodium sulphate (1 g/L) did not significantly decrease MB and CV removal (5%). The adsorption capacity of GO1.5MgO, GO3MgO, GO4.5MgO, and GO6MgO was 95, 248, 280, and 298 mg/g for MB and 53, 198, 199, and 174 mg/g for CV, respectively.

3.2.8. Comparison of different adsorbents

Various materials were synthesized and used as adsorbents for contaminant adsorption [37–45]. Clay nanocomposite (clay/GO/Fe_2O_3) was used for removing methylene blue (19.99 mg/g) [15]. Fe_3O_4 or γ-Fe_2O_3 coated multi-wall

Table 3
Isotherm parameters of dye (MB and CV) adsorption by the synthesized adsorbents (GO1.5MgO, GO3MgO, GO4.5MgO, and GO6MgO)

Dye	Isotherm	Parameter	Adsorbents	Adsorbents	Adsorbents	Adsorbents
			CV-GO1.5MgO	CV-GO3MgO	CV-GO4.5MgO	CV-GO6MgO
CV	Langmuir	Q_0	118	269	268	200
		K_L	0.0294	0.1405	0.0899	0.2578
		R^2	0.8959	0.9958	0.9917	0.9959
	Freundlich	K_F	5	44	30	50
		$1/n$	0.7233	0.5052	0.5755	0.3955
		R^2	0.9473	0.9492	0.9815	0.9172
	Temkin	K_T	0.2592	1.3126	0.7881	2.8009
		B_1	28	59	61	40
		R^2	0.8979	0.9721	0.9765	0.8951
Dye	Isotherm	Parameter	Adsorbents	Adsorbents	Adsorbents	Adsorbents
			MB-GO1.5MgO	MB-GO3MgO	MB-GO4.5MgO	MB-GO6MgO
MB	Langmuir	Q_0	111	286	309	321
		K_L	1.67	2.8443	4.5715	3.4734
		R^2	0.9992	0.9999	0.9999	0.9997
	Freundlich	K_F	96	166	181	191
		$1/n$	0.0295	0.1805	0.2158	0.1901
		R^2	0.8340	0.8001	0.9481	0.5169
	Temkin	K_T	1,213	373	338	539
		B_1	3	30	34	34
		R^2	0.8557	0.8893	0.9427	0.6898

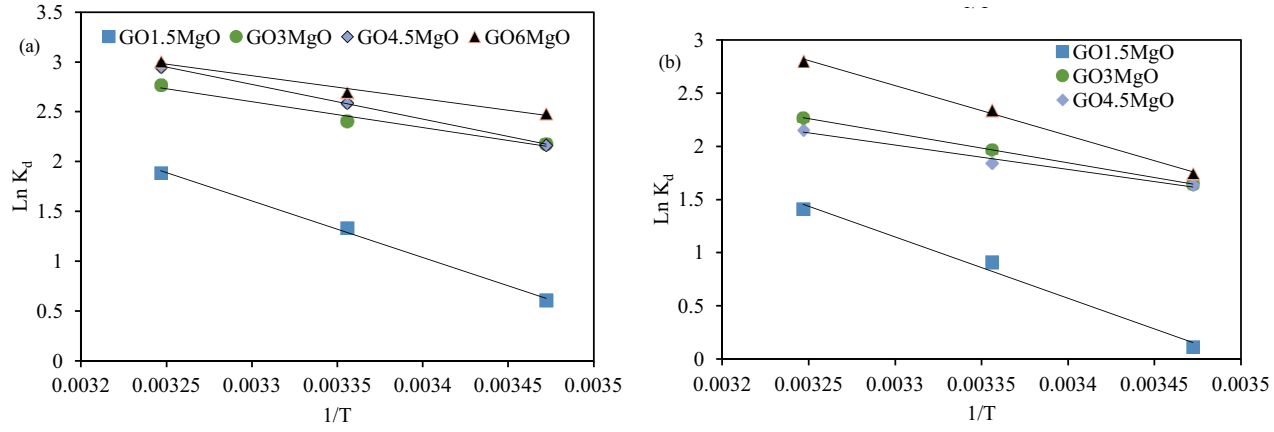

Fig. 10. Thermodynamic of dye adsorption by the synthesized adsorbents (GO1.5MgO, GO3MgO, GO4.5MgO, and GO6MgO) (a) MB and (b) CV.

carbon nanotube was used to remove MB (15.87 mg/g), neutral red (20.51 mg/g), and brilliant cresyl blue (23 mg/g) [16]. Magnetic (γ-Fe_2O_3) sugarcane bagasse activated carbon was used for the adsorption of MB (36 mg/g) [17]. ZnO: Cr-AC was used as an adsorbent of malachite green (MG) (98.36 mg/g), eosin yellow (97.24 mg/g), and auramine O (99.26 mg/g) [18]. The Konjac glucomannan/graphene oxide (KGM/GO) sponge was used to adsorb MG (190 mg/g) [19]. The cobalt iron oxide nanoparticles functionalized hydrazine (CoFeNPs) was used to adsorb amaranth (11 mg/g), naphthol blue black (14 mg/g), acid orange 7 (8 mg/g), reactive orange 16 (68 mg/g), and acid orange 52 (68 mg/g) [20]. In this research, the adsorption ability of the synthesized adsorbents was indicated in Table 5. Dye adsorption capacity of GO and MgO was 108 and 233 mg/g for CV and MB (GO) and 30 and 40 mg/g for CV and MB (MgO), respectively. Also, dye adsorption performance using a commercial activated carbon was carried out as a control group.

Table 4
Thermodynamic parameters of dye (MB and CV) adsorption by the synthesized adsorbents (GO1.5MgO, GO3MgO, GO4.5MgO, and GO6MgO) (T (K), ΔG (J/mol), ΔH (J/mol), and ΔS (J/mol·K)

Adsorbent	T	MB			CV		
		ΔG			ΔG		
GO1.5MgO	288	–1,505.4	R^2	0.9966	–373.6	R^2	0.988
	298	–3,198.4	ΔH	47,253	–2,050.6	ΔH	47,924
	308	–4,891.4	ΔS	169.3	–3,727.6	ΔS	167.7
GO3MgO	288	–5,153	R^2	0.9745	–3,949.2	R^2	0.9999
	298	–6,083	ΔH	21,631	–4,883.2	ΔH	22,950
	308	–7,013	ΔS	93	–5,817.2	ΔS	93.4
GO4.5MgO	288	–5,200.8	R^2	0.9991	–3,865.4	R^2	0.9835
	298	–6,386.8	ΔH	28,956	–4,658.4	ΔH	18,973
	308	–7,572.8	ΔS	118.6	–5,451.4	ΔS	79.3
GO6MgO	288	–5,922.2	R^2	0.9832	–4,219	R^2	0.9973
	298	–6,796.2	ΔH	19249	–5,724	ΔH	39,125
	308	–7,670.2	ΔS	87.4	–7,229	ΔS	150.5

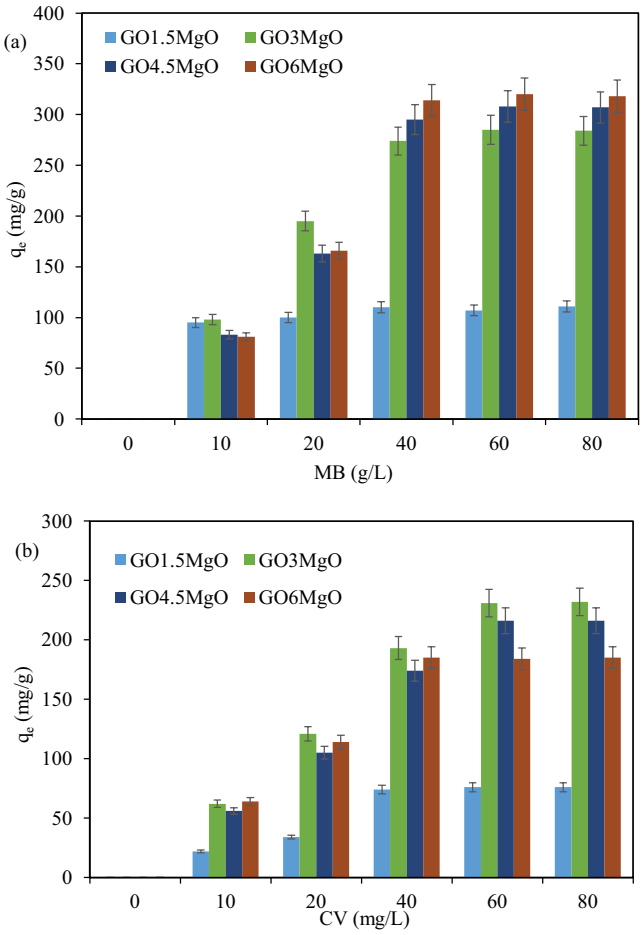

Fig. 11. Pollutant concentration effect on dye adsorption by the synthesized adsorbents (GO1.5MgO, GO3MgO, GO4.5MgO, and GO6MgO) (a) MB and (b) CV.

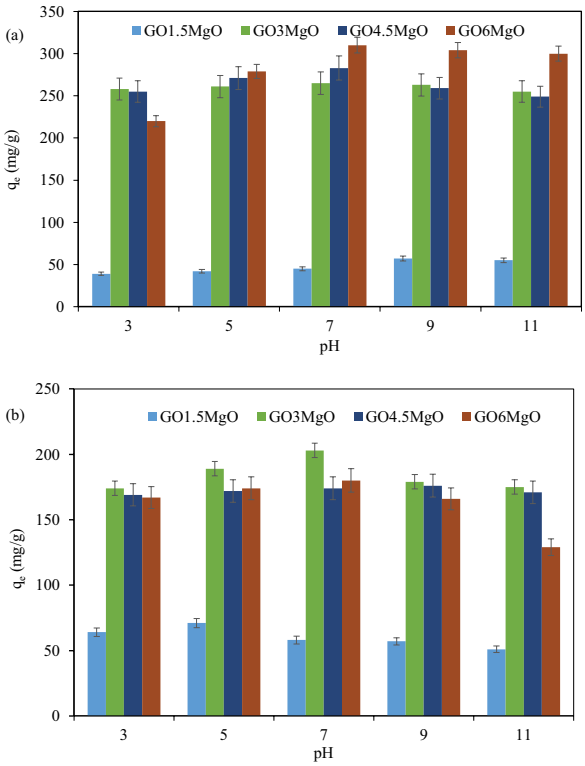

Fig. 12. pH effect on contaminant removal by the synthesized adsorbents (GO1.5MgO, GO3MgO, GO4.5MgO, and GO6MgO) (a) MB and (b) CV.

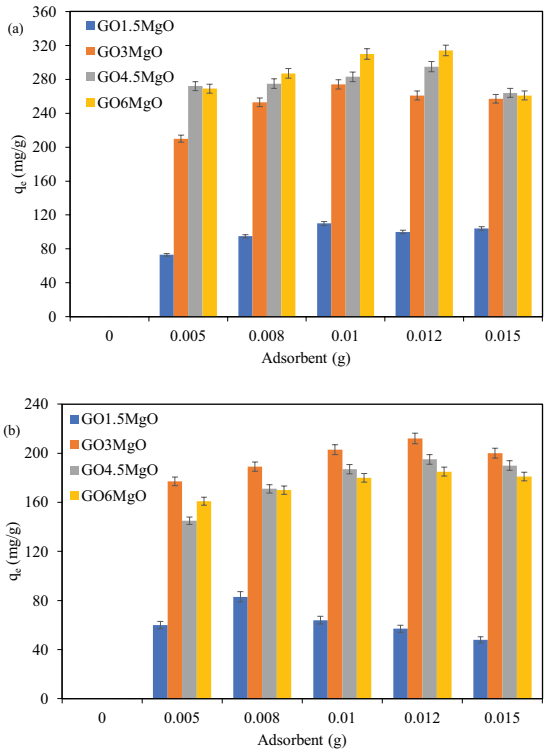

Fig. 13. Adsorbent dosage effect on contaminant adsorption by the synthesized adsorbents (GO1.5MgO, GO3MgO, GO4.5MgO, and GO6MgO) (a) MB and (b) CV.

Table 5
Comparison of the adsorption capacity of different adsorbents

Adsorbent	Dye	Adsorption capacity (mg/g)	References
Clay/GO/Fe_2O_3	Methylene blue	19.99	[15]
	MB	15.87	
Fe_3O_4 or γ-Fe_2O_3 coated multi-walled carbon nanotubes	Neutral red	20.51	[16]
	Brilliant cresyl blue	23	
Magnetic (γ-Fe_2O_3) sugarcane bagasse activated carbon	MB	36	[17]
	Malachite green	98.36	
ZnO: Cr-AC	Eosin yellow	97.24	[18]
	Auramine O	99.26	
Konjac glucomannan/graphene oxide	Malachite green	190	[19]
	Amaranth	11	
Cobalt iron oxide nanoparticles functionalized hydrazine (CoFeNPs)	Naphthol blue black	14	[20]
	Acid orange 7	8	
	Reactive orange 16	68	
	Acid orange 52	68	
GO1.5MgO	Crystal violet (CV)	118	This study
GO1.5MgO	MB	111	
GO3MgO	CV	269	
GO3MgO	MB	286	
GO4.5MgO	CV	268	
GO4.5MgO	MB	309	
GO6MgO	CV	200	
GO6MgO	MB	321	

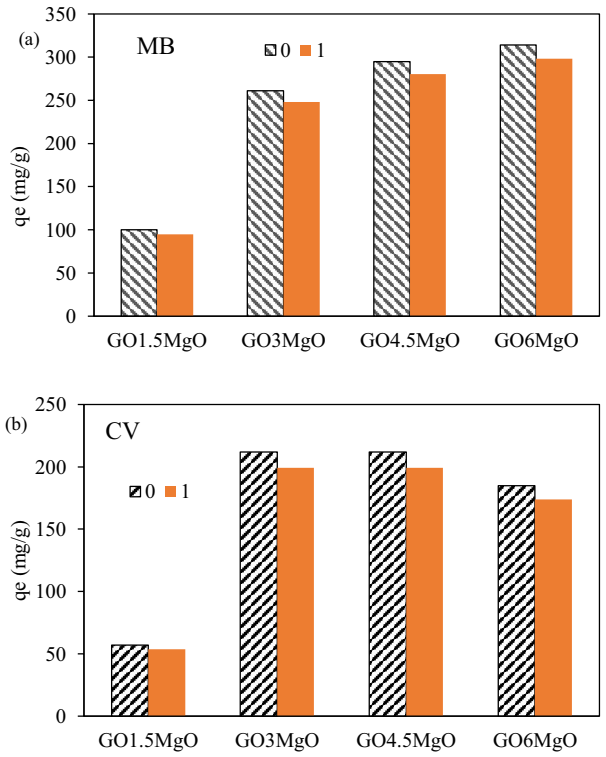

Fig. 14. Salt (sodium sulphate: 0 and 1 g/L) effect on contaminant adsorption by the synthesized adsorbents (GO1.5MgO, GO3MgO, GO4.5MgO, and GO6MgO) (a) MB and (b) CV.

Dye adsorption capacity of commercial activated carbon for CV and MB was 75 and 80 mg/g, respectively. The data presented that GO1.5MgO (CV: 118 and MB: 111), GO3MgO (CV: 269 and MB: 286), GO4.5MgO (CV: 268 and MB: 309), and GO6MgO (CV: 200 and MB: 321) have high removal ability (mg/g) in comparison of other adsorbents.

3.2.9. Regeneration

The adsorbent regeneration is an important parameter for its practical applications. Thus, the regeneration of GO6MgO was studied. The data showed that the GO6MgO recovery efficiency did not decrease considerably after three runs of operations. Adsorption capacity for MB was 321, 312, and 305 mg/g after the three cycles.

4. Conclusion

Herein, graphene oxide–magnesium oxide nanocomposites were synthesized and characterized. Two cationic dyes were used as pollutants. The results presented that the adsorption of MB and CV onto the synthesized adsorbents followed pseudo-second-order. The MB and CV removal by the synthesized adsorbents followed the Langmuir isotherm model in specific homogeneous sites of the adsorbent surface. The negative ΔG value of dye removal indicated physical and spontaneous adsorption. The positive values of ΔH and ΔS, respectively indicate the endothermic properties of adsorption and the increase of dye irregularity on the adsorbent surface. The amount of dye adsorbed on the

synthesized adsorbents increases by increasing the initial contaminant concentration. The results indicated pollutant removal capacity increases by increasing the adsorbent dose (0.005–0.015 g) and then decreases to some extent. As the adsorbent dose increases, the active sites of the adsorbent surface will be more accessible. The adsorbent particles are agglomerated at values higher than the optimal value of the adsorbent dose and dye removal diminished.

References

[1] N.M. Mahmoodi, M. Arami, J. Zhang, Preparation and photocatalytic activity of immobilized composite photocatalyst (titania nanoparticle/activated carbon), J. Alloys Compd., 509 (2011) 4754–4764.

[2] O. Moradi, A. Pudineh, S. Sedaghat, Synthesis and characterization Agar/GO/ZnO NPs nanocomposite for removal of methylene blue and methyl orange as azo dyes from food industrial effluents, Food Chem. Toxicol., 169 (2022) 113412, doi: 10.1016/j.fct.2022.113412.

[3] N.M. Mahmoodi, M. Bashiri, S.J. Moeen, Synthesis of nickel–zinc ferrite magnetic nanoparticle and dye degradation using photocatalytic ozonation, Mater. Res. Bull., 47 (2012) 4403–4408.

[4] O. Moradi, S. Panahandeh, Fabrication of different adsorbents based on zirconium oxide, graphene oxide, and dextrin for removal of green malachite dye from aqueous solutions, Environ. Res., 214 (2022) 114042, doi: 10.1016/j.envres.2022.114042.

[5] N.M. Mahmoodi, F. Moghimi, M. Arami, F. Mazaheri, Silk degumming using microwave irradiation as an environmentally friendly surface modification method, Fibre Polym., 11 (2010) 234–240.

[6] M. Rajabi, K. Mahanpoor, O. Moradi, Removal of dye molecules from aqueous solution by carbon nanotubes and carbon nanotube functional groups: critical review, 7 (2017) 47083–47090.

[7] C. Bauer, P. Jacques, A. Kalt, Photooxidation of an azo dye induced by visible light incident on the surface of TiO_2, J. Photochem. Photobiol., A, 140 (2001) 87–92.

[8] M. Rajabi, B. Mirza, K. Mahanpoor, M. Mirjalili, F. Najafi, O. Moradi, H. Sadegh, R. Shahryari-ghoshekandi, M. Asif, I. Tyagi, S. Agarwal, V.K. Gupta, Adsorption of malachite green from aqueous solution by carboxylate group functionalized multi-walled carbon nanotubes: determination of equilibrium and kinetics parameters, J. Ind. Eng. Chem., 34 (2016) 130–138.

[9] S. Rashmi, B. Bani, Review on decolorisation of aqueous dye solutions by low-cost adsorbents, Color Technol., 118 (2006) 256–69.

[10] O. Moradi, G. Sharma, Emerging novel polymeric adsorbents for removing dyes from wastewater: a comprehensive review and comparison with other adsorbents, Environ. Res., 201 (2021) 111534, doi: 10.1016/j.envres.2021.111534.

[11] S. Agarwal, I. Tyagi, V.K. Gupta, F. Golbaz, A.N. Golikand, O. Moradi, Synthesis and characteristics of polyaniline/zirconium oxide conductive nanocomposite for dye adsorption application, J. Mol. Liq., 218 (2016) 494–498.

[12] N.C. Joshi, P. Gururani, Advances of graphene oxide-based nanocomposite materials in the treatment of wastewater containing heavy metal ions and dyes, Curr. Res. Green Sustainable Chem., 5 (2022) 100306, doi: 10.1016/j.crgsc.2022.100306.

[13] K.S. Novoselov, V.I. Fal'ko, L. Colombo, P.R. Gellert, M.G. Schwab, K. Kim, A roadmap for graphene, Nature, 490 (2012) 192–200.

[14] A. Moghadam, M.S. Mobarakeh, M. Safaei, S. Kariminia, Synthesis and characterization of novel bio-nanocomposite of polyvinyl alcohol-Arabic gum-magnesium oxide via direct blending method, Carbohydr. Polym., 260 (2021) 117802, doi: 10.1016/j.carbpol.2021.117802.

[15] N. Farooq, M.I. Khan, A. Shanableh, A.M. Qureshi, S. Jabeen, A. ur Rehman, Synthesis and characterization of clay graphene oxide iron oxide (clay/GO/Fe_2O_3)-nanocomposite for adsorptive removal of methylene blue dye from wastewater, Inorg. Chem. Commun., 145 (2022) 109956, doi: 10.1016/j.inoche.2022.109956.

[16] J.L. Gong, B. Wang, G.M. Zeng, C.P. Yang, C.G. Niu, Q.Y. Niu, W.J. Zhou, Y. Liang, Removal of cationic dyes from aqueous solution using magnetic multi-wall carbon nanotube nanocomposite as adsorbent, J. Hazard. Mater., 164 (2009) 1517–1522.

[17] W. Jiang, L. Zhang, X. Guo, M. Yang, Y. Lu, Y. Wang, Y. Zheng, G. Wei, Adsorption of cationic dye from water using an iron oxide/activated carbon magnetic composites prepared from sugarcane bagasse by microwave method, Environ. Technol., 42 (2021) 337–350.

[18] M. Jamshidi, M. Ghaedi, K. Dashtian, S. Hajati, A.A. Bazrafshan, Sonochemical assisted hydrothermal synthesis of ZnO: Cr nanoparticles loaded activated carbon for simultaneous ultrasound-assisted adsorption of ternary toxic organic dye: derivative spectrophotometric, optimization, kinetic and isotherm study, Ultrason. Sonochem., 32 (2016) 119–131.

[19] T. Chen, P. Shi, J. Zhang, Y. Li, T. Duan, L. Dai, L. Wang, X. Yu, W. Zhu, Natural polymer konjac glucomannan mediated assembly of graphene oxide as versatile sponges for water pollution control, Carbohydr. Polym., 202 (2018) 425–433.

[20] Q. Ain, S. Khurshid, Z Gul, J. Khatoon, M.R. Shah, I. Hamid, I.A.T. Khan, F. Aslam, Anionic azo dyes removal from water using amine functionalized cobalt-iron oxide nanoparticles: a comparative time-dependent study and structural optimization towards the removal mechanism, RSC Adv., 10 (2019) 1021–1041.

[20] V. Loryuenyong, K. Totepvimarn, P. Eimburanapravat, W. Boonchompoo, A. Buasri, Preparation and characterization of reduced graphene oxide sheets via water-based exfoliation and reduction methods, Adv. Mater. Sci. Eng., 2013 (2013) 923403, doi: 10.1155/2013/923403.

[21] X. Su, G. Wang, W. Li, J. Bai, H. Wang, A simple method for preparing graphene nano-sheets at low temperature, Adv. Powder Technol., 24 (2013) 317–323.

[22] H. Zhang, X. Wang, N. Li, J. Xia, Q. Meng, J. Ding, J. Lu, Synthesis and characterization of TiO_2/graphene oxide nanocomposites for photoreduction of heavy metal ions in reverse osmosis concentrate, RSC Adv., 8 (2018) 34241–34251.

[23] L. Kashinath, K. Namratha, K. Byrappa, Sol-gel assisted hydrothermal synthesis and characterization of hybrid ZnS-RGO nanocomposite for efficient photodegradation of dyes, J. Alloys Compd., 695 (2017) 799–809.

[24] Z. Fan, K. Wang, T. Wei, J. Yan, L. Song, B. Shao, An environmentally friendly and efficient route for the reduction of graphene oxide by aluminum powder, Carbon, 48 (2010) 1686–1689.

[25] M. El Achaby, F.Z. Arrakhiz, S. Vaudreuil, E.M. Essassi, A. Qaiss, Piezoelectric β-polymorph formation and properties enhancement in graphene oxide—PVDF nanocomposite films, Appl. Surf. Sci., 258 (2012) 7668–7677.

[26] A. Bagri, C. Mattevi, M. Acik, Y.J. Chabal, M. Chhowalla, V.B. Shenoy, Structural evolution during the reduction of chemically derived graphene oxide, Nat. Chem., 2 (2010) 581–587.

[27] G. Crini, P.M. Badot, Application of chitosan, a natural aminopolysaccharide, for dye removal from aqueous solutions by adsorption processes using batch studies: a review of recent literature, Prog. Polym. Sci., 33 (2008) 399–447.

[28] B. Hayati, N.M. Mahmoodi, A. Maleki, Dendrimer–titania nanocomposite: synthesis and dye-removal capacity, Res. Chem. Intermed., 41 (2015) 3743–3757.

[29] N.M. Mahmoodi, Dendrimer functionalized nanoarchitecture: synthesis and binary system dye removal, J. Taiwan Inst. Chem. Eng., 45 (2014) 2008–2020.

[30] F. Hosseini, S. Sadighian, H. Hosseini-Monfared, N.M. Mahmoodi, Dye removal and kinetics of adsorption by

magnetic chitosan nanoparticles, Desal. Water Treat., 57 (2016) 24378–24386.
[31] N.M. Mahmoodi, F. Najafi, Synthesis, amine functionalization and dye removal ability of titania/silica nano-hybrid, Microporous Mesoporous Mater., 156 (2012) 153–160.
[32] B. Hayati, N.M. Mahmoodi, M. Arami, F. Mazaheri, Dye removal from colored textile wastewater by poly (propylene imine) dendrimer: operational parameters and isotherm studies, Clean – Soil, Air, Water, 39 (2011) 673–679.
[33] N.M. Mahmoodi, Dendrimer functionalized nanoarchitecture: synthesis and binary system dye removal, J. Taiwan Inst. Chem. Eng., 45 (2014) 2008–2020.
[34] A. Almasian, M.E. Olya, N.M. Mahmoodi, Preparation and adsorption behavior of diethylenetriamine/polyacrylonitrile composite nanofibers for a direct dye removal, Fibre Polym., 16 (2015) 1925–1934.
[35] O. Moradi, Applicability comparison of different models for ammonium ion adsorption by multi-walled carbon nanotube, Arabian J. Chem., 9 (2016) S1170–S1176.
[36] A. Almasian, N.M. Mahmoodi, M.E. Olya, Tectomer grafted nanofiber: synthesis, characterization and dye removal ability from multicomponent system, J. Ind. Eng. Chem., 32 (2015) 85–98.
[37] N.M. Mahmoodi, Nickel ferrite nanoparticle: synthesis, modification by surfactant and dye removal ability, Water Air Soil Pollut., 224 (2013) 1419, doi: 10.1007/s11270-012-1419-7.
[38] C. Nanthamathee, P. Dechatiwongse, Kinetic and thermodynamic studies of neutral dye removal from water using zirconium metal-organic framework analogues, Mater. Chem. Phys., 258 (2021) 123924, doi: 10.1016/j.matchemphys.2020.123924.
[39] N.M. Mahmoodi, B. Hayati, M. Arami, Kinetic, equilibrium and thermodynamic studies of ternary system dye removal using a biopolymer, Ind. Crops Prod., 35 (2012) 295–301.
[40] A.M. Rheima, A.A. Khadom, M.M. Kadhim, Removal of Cibacron Blue P-6B dye from aqueous solution using synthesized anatase titanium dioxide nanoparticles: thermodynamic, kinetic, and theoretical investigations, J. Mole. Liq., 357 (2022) 119102, doi: 10.1016/j.molliq.2022.119102.
[41] M.I. El-Khaiary, G.F. Malash, Common data analysis errors in batch adsorption studies, Hydrometallurgy, 105 (2011) 314–320.
[42] E.C. Lima, F. Sher, A. Guleria, M.R. Saeb, I. Anastopoulos, H.N. Tran, A. Hosseini-Bandegharaei, Is one performing the treatment data of adsorption kinetics correctly?, J. Environ. Chem. Eng., 9 (2021) 104813, doi: 10.1016/j.jece.2020.104813.
[43] K.Y. Foo, B.H. Hameed, Insights into the modeling of adsorption isotherm systems, Chem. Eng. J., 156 (2010) 2–10.
[44] H.N. Tran, S.J. You, A. Hosseini-Bandegharaei, H.P. Chao, Mistakes and inconsistencies regarding adsorption of contaminants from aqueous solutions: a critical review, Water Res., 120 (2017) 88–116.
[45] K.L. Tan, B.H. Hameed, Insight into the adsorption kinetics models for the removal of contaminants from aqueous solutions, J. Taiwan Inst. Chem. Eng., 74 (2017) 25–48.

Supporting information

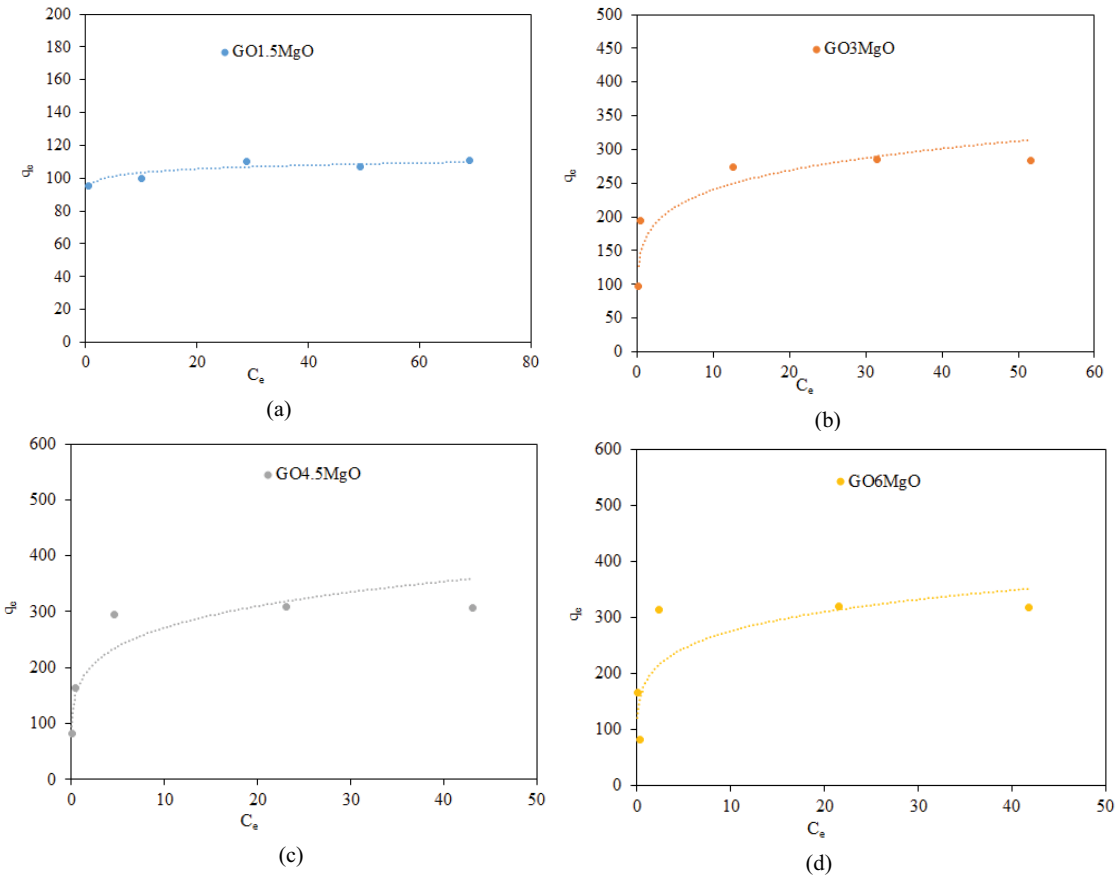

Fig. S1. Non-linear Langmuir isotherm of MB adsorption by the synthesized adsorbents (a) GO1.5MgO, (b) GO3MgO, (c) GO4.5MgO, and (d) GO6MgO.

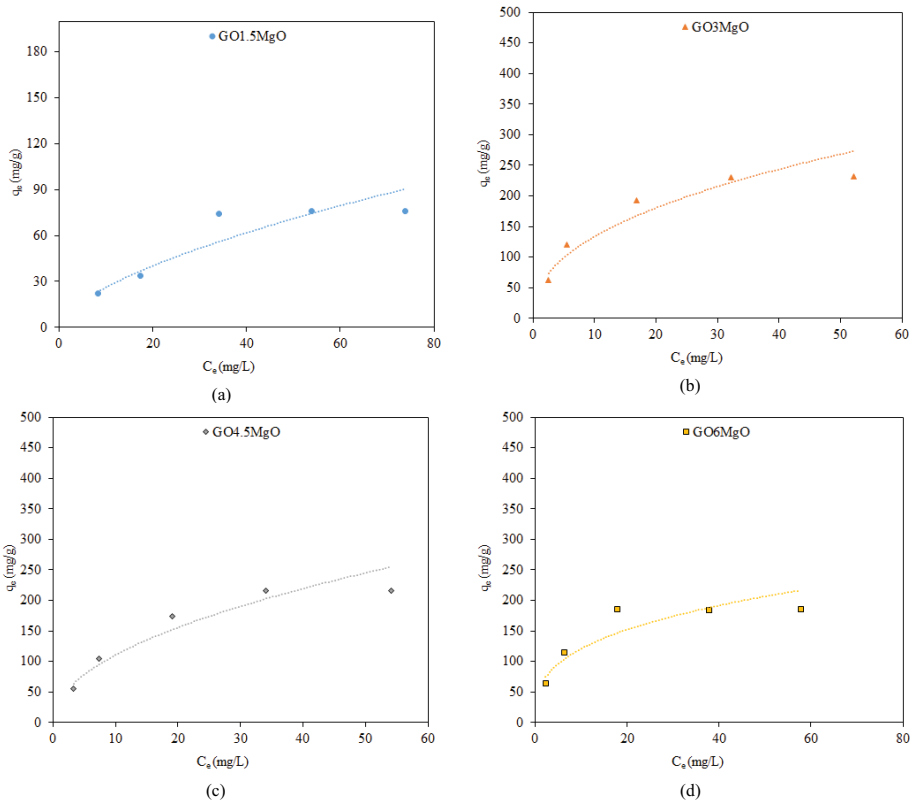

Fig. S2. Non-linear Langmuir isotherm of CV adsorption by the synthesized adsorbents (a) GO1.5MgO, (b) GO3MgO, (c) GO4.5MgO, and (d) GO6MgO.

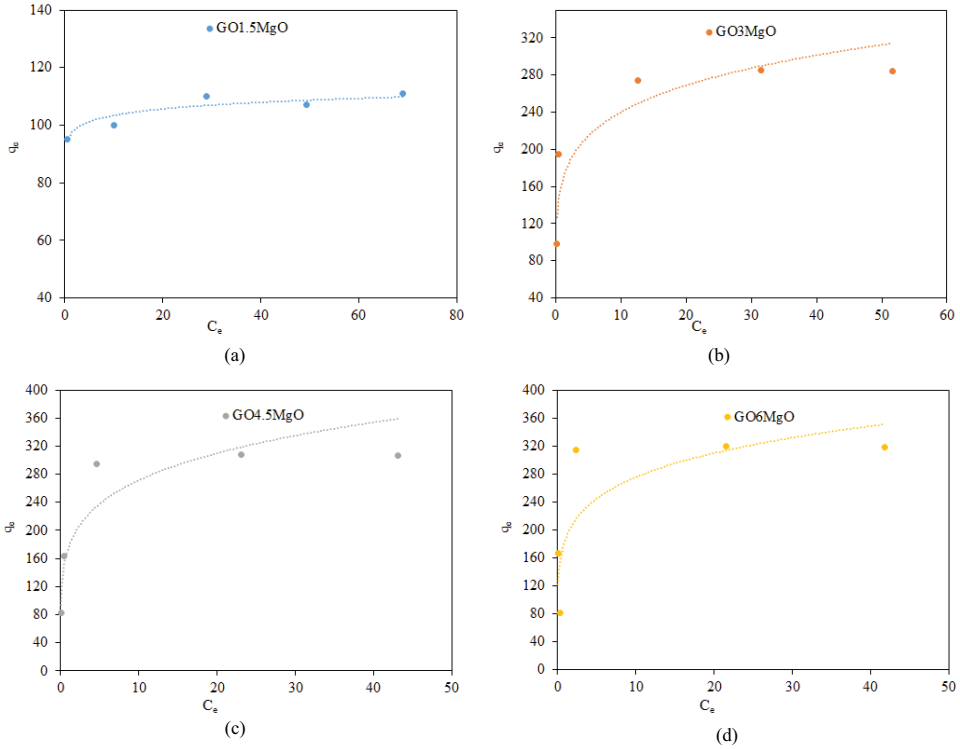

Fig. S3. Non-linear Freundlich isotherm of MB adsorption by the synthesized adsorbents (a) GO1.5MgO, (b) GO3MgO, (c) GO4.5MgO, and (d) GO6MgO.

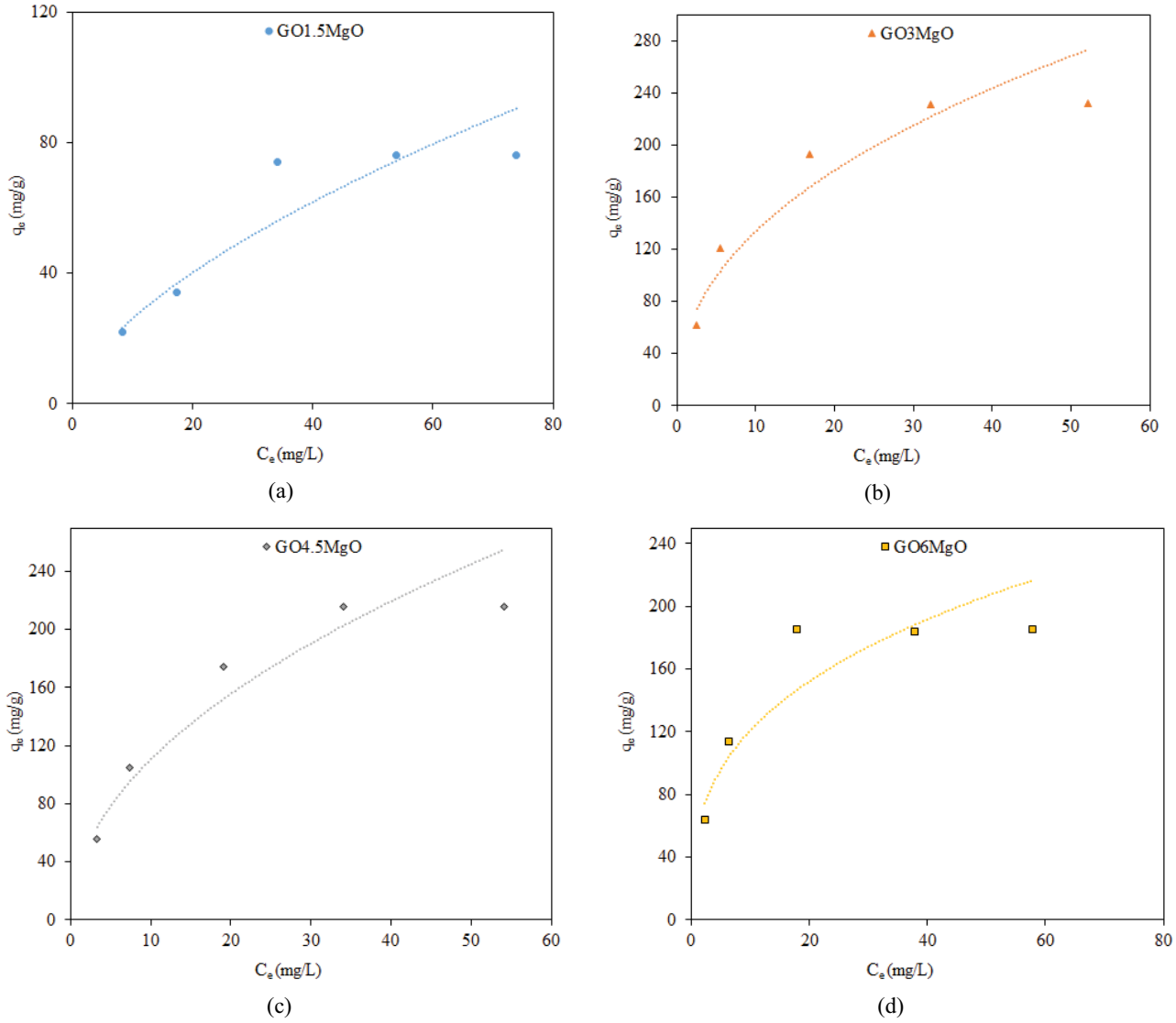

Fig. S4. Non-linear Freundlich isotherm of CV adsorption by the synthesized adsorbents (a) GO1.5MgO, (b) GO3MgO, (c) GO4.5MgO, and (d) GO6MgO.

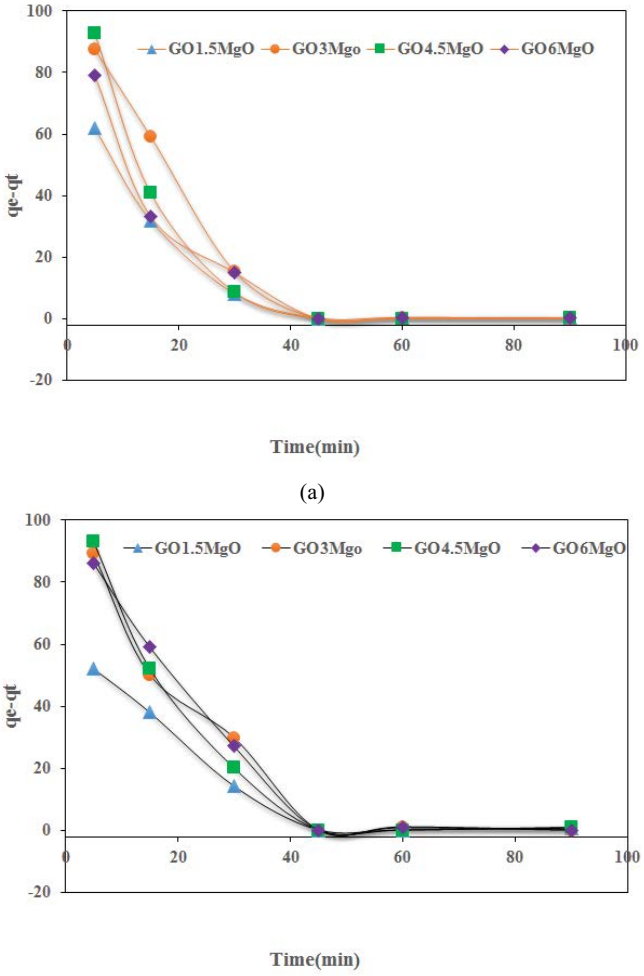

Fig. S5. Non-linear pseudo-first-order of dye adsorption by the synthesized adsorbents (GO1.5MgO, GO3MgO, GO4.5MgO, and GO6MgO) (a) MB and (b) CV.

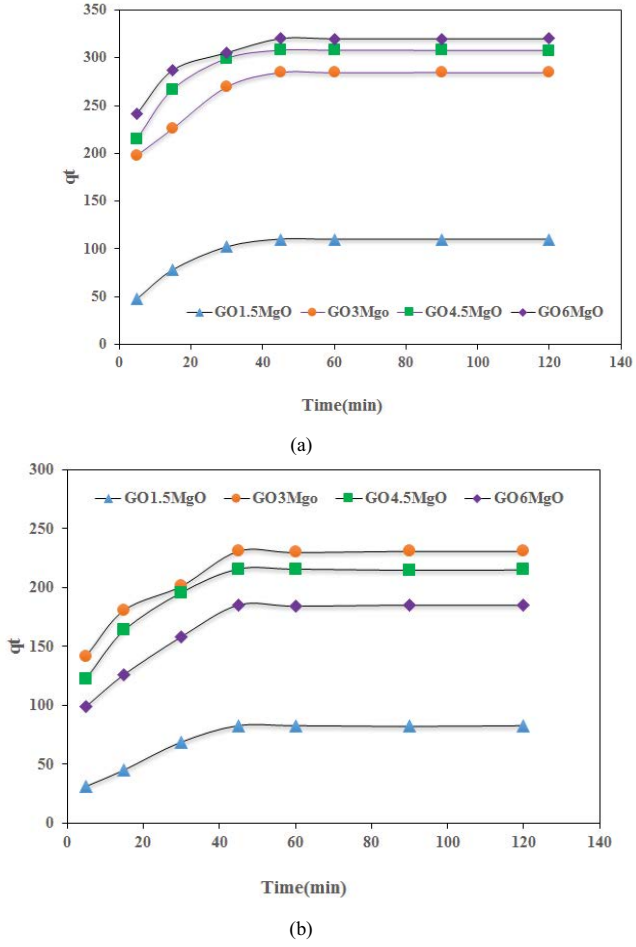

Fig. S6. Non-linear pseudo-second-order of dye adsorption by the synthesized adsorbents (GO1.5MgO, GO3MgO, GO4.5MgO, and GO6MgO) (a) MB and (b) CV.

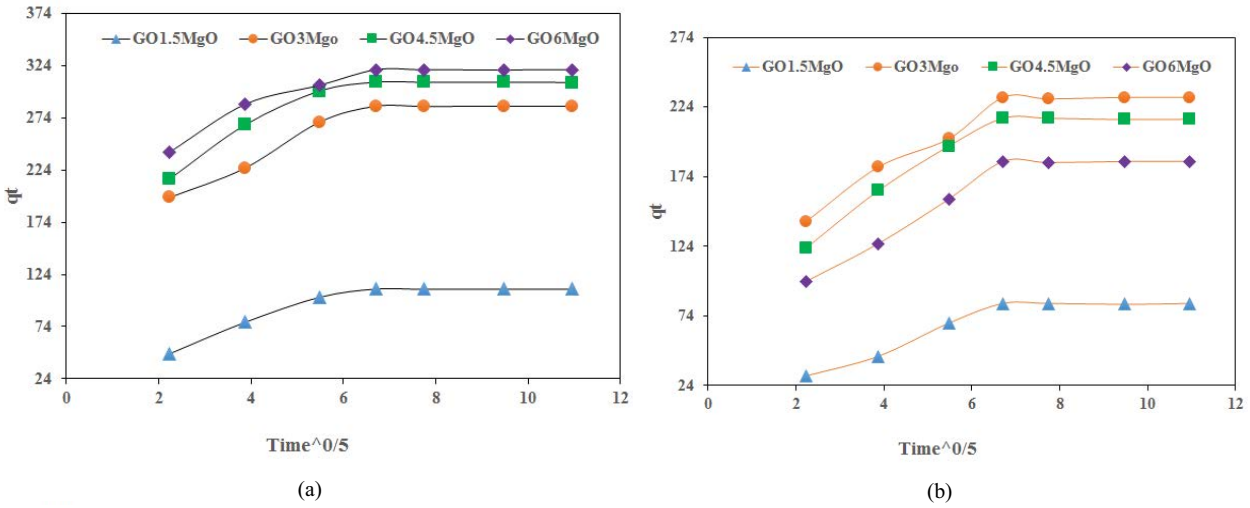

Fig. S7. Intraparticle diffusion of dye adsorption by the synthesized adsorbents (GO1.5MgO, GO3MgO, GO4.5MgO, and GO6MgO) (a) MB and (b) CV.